Charged-cell periodic DFT simulations via an impurity model based on density embedding: Application to the ionization potential of liquid water

André Severo Pereira Gomes, Johannes Tölle, Andre Severo, Pereira Gomes, Pablo Ramos, Michele Pavanello

Proper Charged-cell Periodic DFT Simulations Via an Impurity Model Based on Density Embedding

Johannes Tölle,[1,2] Andre Severo Pereira Gomes,[3,a)] Pablo Ramos,[1] and Michele Pavanello[1,b)]

[1)] *Department of Chemistry, Rutgers University, Newark, NJ 07102, USA*

[2)] *Theoretische Organische Chemie, Organisch-Chemisches Institut and Center for Multiscale Theory and Computation (CMTC), Westfälische Wilhelms-Universität Münster, Corrensstrasse 40, 48149 Münster, Germany*

[3)] *Université de Lille, CNRS, UMR 8523 PhLAM Physique des Lasers, Atomes et Molécules, F-59000 Lille, France*

Calculations of charged systems in periodic boundary conditions are problematic because there are spurious interactions between the charges in different periodic images that can affect the physical picture. In addition, the intuitive limit of Coulomb interactions decaying to zero as the interacting charges are placed at infinite separation no longer applies, and for example total energies become undefined. Leveraging subsystem DFT (also known as density embedding) we define an appropriate impurity model that embeds a finite neutral or charged subsystem within an extended (infinite) surrounding subsystem. The combination of the impurity model and an appropriate, consistent choice of the Coulomb reference provides us with an algorithm for evaluating the ionization potential of liquid water. We obtain an average vertical IP for liquid water of 10.5 eV, which compares favorably with experiments (9.9–10.06 eV) and very recent simulations based on the GW approximation (10.55 eV). In addition, our calculations show that the IP distribution of liquid water is much broader than the one of gas phase water. This is plausible, and we find it to be similar to the comparison of the optical spectrum of liquid and gas phase water.

[a)]Electronic mail: andre.gomes@univ-lille1.fr

[b)]Electronic mail: m.pavanello@rutgers.edu

I. INTRODUCTION

Atomistic models of extended systems (such as solids and liquids) typically prescribe the use of periodic boundary conditions (PBC). Once PBC are invoked, Coulomb interactions should no longer be evaluated in real space. Namely, if $\mathbf{r}, \mathbf{r}' \in \mathbb{R}^3$ then Coulomb kernel for a finite system is $w(\mathbf{r}, \mathbf{r}') = \frac{1}{|\mathbf{r}-\mathbf{r}'|}$. When working in PBC, instead, Coulomb interactions should be evaluated in reciprocal space. Namely, $\mathbf{G} \in \mathbb{R}^3$ then Coulomb kernel becomes $w(\mathbf{G}) = \frac{4\pi}{|\mathbf{G}|^2}$. The physical behavior of the kernel is to decay to zero when the interacting charges are at an infinite distance from each other. However, in PBC distance is not a well defined quantity[1] and the physical kernel is only the one represented in reciprocal space.

This does not seem to be problematic because, although $\frac{4\pi}{|\mathbf{G}|^2}$ is singular for $\mathbf{G} = 0$, the total charge density $\rho(\mathbf{G})$ is zero for $\mathbf{G} = 0$. The neutrality of the charge density is the only physical choice in PBC, because otherwise one would need to admit an infinitely-charged system in the realm of the physical world. Clearly, it is not possible.

In practical calculations, PBC are often employed even if the systems of interest is not be periodic *per se* simply as a matter of convenience. For example, this occurs in DFT simulations of defects, where the physical system is intrinsicly nonperiodic[2]. However, due to the practical advantages of simulating only a small simulation cell, leading to manageable computational requirements, has led to considering employing PBC even for simulating charged systems (i.e., systems where the electronic and the nuclear charges do not cancel out). Two avenues have been so far explored to allow such a model: (1) Correcting the potential so that its long-ranged part is truncated at the boundaries of the simulation cell making use of numerical Fourier transforms with the minimum image convention[3], or aligning the potential averages in the bulk with the one of semi-infinite versions of the system allowing, e.g., comparison of electronic band energies[4–10] ; and (2) adding a "neutralizing" constant background charge density. The latter has several drawbacks. Energies need to be corrected[11–14] due to the inherent tin-foil boundary conditions chosen (i.e., the fact that adding a neutralizing background charge is equivalent to wrapping the almost infinitely extended system by a conductor that nullifies the average potential inside the system) .

In this work, we present an impurity model with the following important qualities:

- The charged periodic system is replaced by a nonperiodic one which is still truly extended (i.e., of infinite size).

- The potentials of the neutral and the charged systems are pegged to a common reference.

While achieving the latter simply requires finding an appropriate choice for the $\mathbf{G} = 0$ component of the Coulomb kernel, achieving the former requires an *ad hoc* mapping of the infinite system onto a collection of finite subsystems and an extended (infinite) subsystem. Thus, in formulating such a map we will make use of a formally exact density embedding method, subsystem DFT[15].

II. THEORETICAL BACKGROUND

A. Mapping an extended system onto a collection of finite subsystems and one extended subsystem

Consider a supersystem composed of two subsystems one being finite with charge density ρ_I for which the Coulomb potential can be safely defined in real space, and the other with charge density $\rho - \rho_I$ with ρ being fully periodic on a given lattice.

The total electron density is then taken to be the sum of the finite subsystem and the extended subsystem

$$\rho(\mathbf{r}) = \rho_I(\mathbf{r}) + \Big(\rho(\mathbf{r}) - \rho_I(\mathbf{r})\Big). \tag{1}$$

Following the prescrition of subsystem DFT, the total energy is given by

$$E_{\text{tot}} = E[\rho_I] + E[\rho - \rho_I] + E^{int}[\rho_I, \rho - \rho_I] \tag{2}$$

The interaction energy can be decomposed as follows[15–17]

$$E^{int} = E_H^{int} + V_{eN}^{int} + T_s^{nad} + E_{xc}^{nad}, \tag{3}$$

where the two Coulombic terms, E_H^{int} and V_{eN}^{int}, regard electron–electron and electron–nuclear interactions, respectively; the nonadditive terms, T_s^{nad} and E_{xc}^{nad}, represent interactions related among others to exchange, van der Waals and Pauli repulsion and are all bifunctionals of the two subsystem densities[18].

In the following, we consider ways to evaluate the interaction part of the energy expression. This is the term that requires most care, as ρ_I may be the density of a charged system[19].

B. Evaluating the Coulomb part of E^{int}

For sake of simplicity, we treat here only the Hartree term of the interaction energy. The electron–nuclear interaction can be treated in an equivalent way. The Hartree interaction energy between the finite and the infinite electronic systems is given by

$$E_H^{int} = \int_{\mathbb{R}^3} \mathrm{d}\mathbf{r} \int_{\Omega} \mathrm{d}\mathbf{r}' \; \frac{1}{|\mathbf{r}-\mathbf{r}'|} \Big[\rho(\mathbf{r}) - \rho_I(\mathbf{r})\Big] \rho_I(\mathbf{r}'). \tag{4}$$

The integral in $\mathrm{d}\mathbf{r}$ is carried out over the entire space because the density $\rho - \rho_I$ is extended. Conversely, the integral over $\mathrm{d}\mathbf{r}'$ is carried out only over a finite volume Ω (typically the simulation cell) because we expect $\rho_I(\mathbf{r}) = 0$ when $\mathbf{r} \notin \Omega$.

We thus have two simingly equivalent methods to compute the interaction.

1. Method I: Finite potential interacting with a periodic charge

Defining the finite potential (denoted by an overbar) as being the potential with ρ_I as source, we find

$$\bar{v}[\rho_I](\mathbf{r}) = \int_{\Omega} \mathrm{d}\mathbf{r}' \; \frac{1}{|\mathbf{r}-\mathbf{r}'|} \rho_I(\mathbf{r}'), \tag{5}$$

where, once again, there is no need to extend the domain of integration to outside Ω because the integrand is identically zero outside the Ω domain.

The interaction becomes:

$$E_H^{int} = \int_{\mathbb{R}^3} \mathrm{d}\mathbf{r} \; \bar{v}[\rho_I](\mathbf{r}) \Big[\rho(\mathbf{r}) - \rho_I(\mathbf{r})\Big]. \tag{6}$$

The inconvenience is the need to represent the finite potential, $\bar{v}[\rho_I](\mathbf{r})$, also outside Ω. However, The following approximate expression for the interaction can be employed in practical calculations

$$E_H'^{\,int}(\Omega') = \int_{\Omega'} \mathrm{d}\mathbf{r} \; \bar{v}[\rho_I](\mathbf{r}) \Big[\rho(\mathbf{r}) - \rho_I(\mathbf{r})\Big]. \tag{7}$$

In this sense, Ω' can be used as a convergence parameter because of the following limit,

$$\lim_{\Omega' \to \mathbb{R}^3} E_H'^{\,int}(\Omega') = E_H^{int}. \tag{8}$$

In practical calculations, we expect to require only Ω' of manageable, sizes. For example, $\Omega' = \Omega$, the simulation cell. This leads to fast algorithms as the potential outside Ω is smooth and can be represented on extremely coarse grids[20].

In principle, the value of the limit in Eq. (8) depends on how the limit is taken due to the conditional convergence of the integral in Eq. (7). However, it generally leads to a term linear in the charge density involving dipole and quadrupole terms[3,4,14,21–23].

2. *Method II: Periodic potential interacting with a finite charge*

An alternative way is to compute the potential generated by the periodic system and use that in the computation of E_{int},

$$E_{int} = \int_{\Omega} \mathrm{d}\mathbf{r} \left[v[\rho](\mathbf{r}) - \bar{v}[\rho_I](\mathbf{r}) \right] \rho_I(\mathbf{r}). \tag{9}$$

Although this may seem equivalent to the previous case, there is an ambiguity because the boundary conditions employed to solve the Poisson equation for the $\rho \to v[\rho](\mathbf{r})$ differ from the ones employed in $\rho_I(\mathbf{r}) \to \bar{v}[\rho_I](\mathbf{r})$.

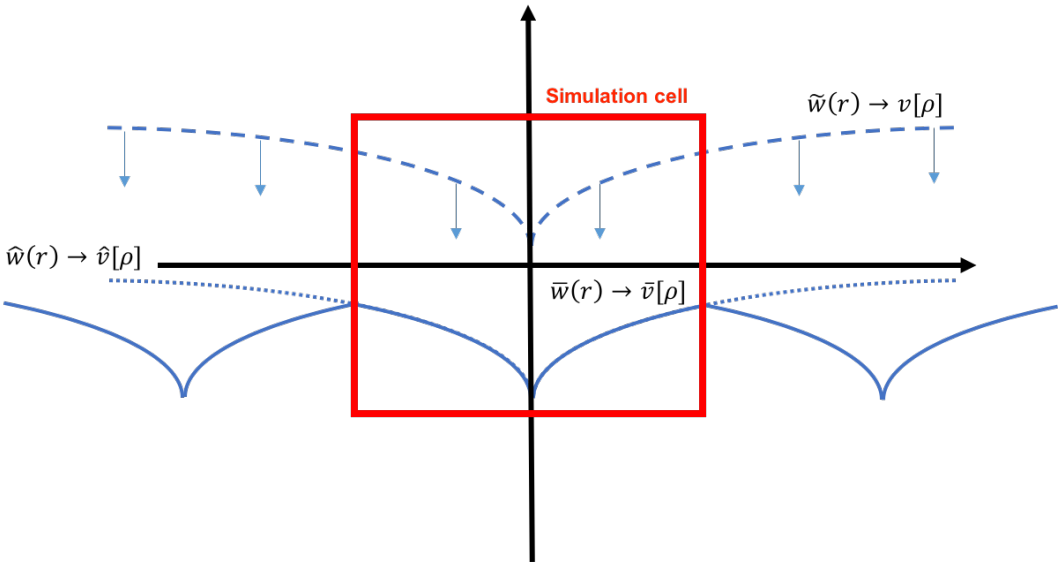

FIG. 1. Dashed line: Coulomb kernel of the periodic system. The Coulomb interaction extrends outside the simulation cell with the characteristic $\frac{1}{r}$ decay. Full line: Coulomb kernel of the finite system which periodically repeats itself so that interactions between spurious periodic images of the finite charge density are completely removed[3]. Dotted line: the Coulomb kernel for the periodic system referenced to the same $\mathbf{G} = 0$ value as the nonperiodic one. In this way, interaction energies computed with the periodic and the nonperiodic kernels are compatible.

In this work, we circumvent the above ambiguity by imposing the $\mathbf{G} = 0$ value of the

periodic Coulomb kernel to match the same limit of the Coulomb kernel of a reference system (see Figure 1). As of Figure 1 suggests, the reference system can be a finite subsystem, or it can be another system for which total energies or interactions are compared against.

In all calculations presented in this work, we employ Method II. As we will report on ionization potentials, it is enough for us to refer the periodic potential to have the same $\mathbf{G} = 0$ component for the potential for the $\rho - \rho_I$ subsystem in the ionized and neutral species.

C. Mapping an impurity

Let us now imagine that a subsystem, say J, undergoes some sort of chemical transformation only at one lattice point while all other lattice points have ρ_J. That is:

$$\begin{aligned} &\rho_J(\mathbf{r}) \rightarrow \text{Chemical Transformation} &&\rightarrow \rho'_J(\mathbf{r}) \text{ at one lattice point,} \\ &\rho_J(\mathbf{r}) \rightarrow \text{No Transformation} &&\rightarrow \rho_J(\mathbf{r}) \text{ anywhere else.} \end{aligned}$$

We call ρ'_J an **impurity**.

The Coulomb potential of an impurity can then be computed by the application of a new screening potential, Δv^{screen} to the periodic Coulomb potential of the impurity calculation. Namely,

$$\Delta v^{\text{screen}}[\rho_J, \rho'_J](\mathbf{r}) = v^{\text{screen}}[\rho_J](\mathbf{r}) - v^{\text{screen}}[\rho'_J](\mathbf{r}), \tag{10}$$

where

$$v^{\text{screen}}[\rho_J](\mathbf{r}) = v[\rho_J](\mathbf{r}) - \bar{v}[\rho_J](\mathbf{r}), \tag{11}$$

where once again we indicate with an overbar the potential evaluated with the Coulomb kernel in real space. In practical calculations, as we still make use of an auxiliary reciprocal space, we adopt the method by Martyna and Tuckerman[3].

Δv^{screen} can be understood as a screening function which replaces the environment of impurity charge densities, ρ'_J with an environment of pristine ρ_J.

For example, when the *chemical transformation* is an ionization, Δv^{screen} replaces the electrostatic environment given by periodic images of the ionized subsystem J with the nonionized (neutral) ρ_J surrounding. This is the essential feature of the proposed method – that is, using the screening potentials in Eq.(11), we can effectively create an impurity within an extended system.

In practical calculations, this procedure is carried out only semi-selfconsistently. This is because $v^{\text{screen}}[\rho_J]$ is imported from a calculation without impurity and v^{screen} is instead calculated at every selfconsistent field (SCF) step. In the results section, we present values obtained with selfconsistent screening and also with static screening computed only for the neutral system and kept static also when computing the impurity.

In the following we first list the computationl details of our calculations, then we show an example of impurity calculation of a single water molecule embedded in a lattice of replicas of itself repeated by the imposed periodic boundary conditions. Finally, we carry out a pilot calculation to showcase our method and compute the ionization potential of bulk water by selecting a single snapshot of a subsystem DFT based molecular dynamics of water 64 (64 water molecules, each being one subsystem inside a simulation cell in PBC) averaging over the set of 64 water molecules. We then close with a conclusion and future direrctions section.

III. COMPUTATIONAL DETAILS

All calculations were carried out with embedded Quantum ESPRESSO[24] and were run at the Γ-point employing ultrasoft pseudopotentials (pbe-rrkjus.UPF from the main Quantum-Espresso pseudopotential library), 40Ry and 400Ry are the energy cutoffs for the plane wave expansions of the molecular orbitals and the charge density, respectively.

Each water molecule considered was treated as one subsystem. The periodic box used for the plane wave expansion of each subsystem was customized to have a lattice vector which is 60% of that of the native box for water 64. This allowed us to reduce the number of plane waves to expand the waves of each water molecule from 55,000 to 12,000.

We use the PBE exchange–correlation functional[25] for the additive and nonadditive contributions to the energy, and the revAPBEK[26] nonadditive Kinetic energy functional.

IV. RESULTS AND DISCUSSION

A. An impurity gedanken experiment

As depicted in Figure 2, the impurity model prescribes combining the water molecule system as if it was a finite system (i.e., no PBC) and subtracting the Coulomb potential due

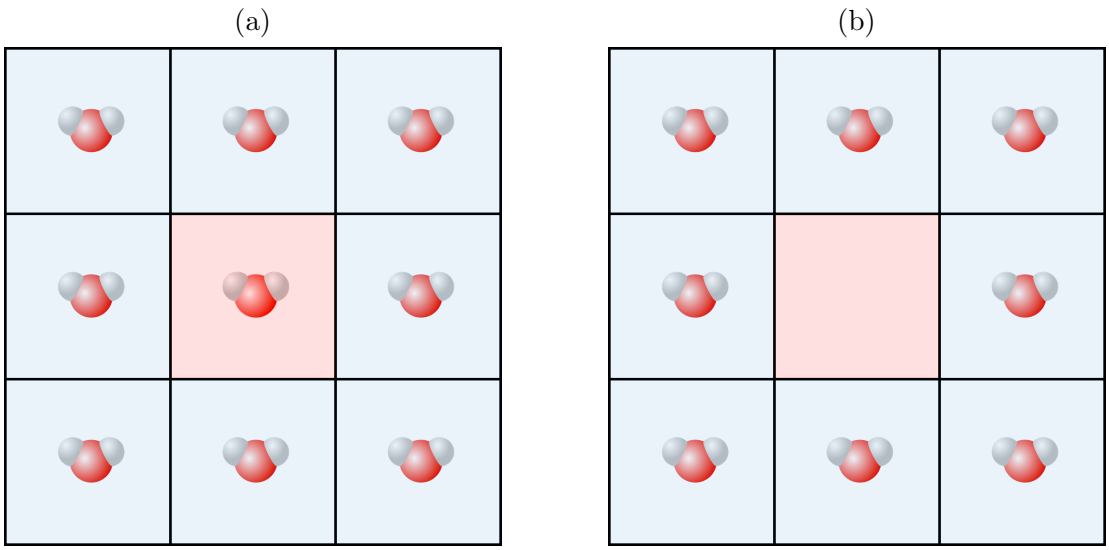

FIG. 2. Depiction of the gedanken experiment by which a single water molecule is placed in the center of a cubic simulation cell (squares). The simulation is carried out in PBC, thus in inset (a) there are replicas of such a water molecule everywhere in space as denoted by the blue squares. The impurity model is depicted in inset (b).

to this water molecule from the Coulomb potential of the same water treated in PBC.

This gedanken experiment is carried out to provide the reader with an appreciation for the screening potential [defined in Eq. (11)] and its features. Figure 3 depicts the screening potential associated with a single water molecule in a cubic simulation cell which is found to have the shape of a dipole potential exerted by the surrounding periodic images onto the impurity site.

The screening potential can be thought of as the electrostatic potential of the periodically repeating water molecules have on a single lattice site. That is, the empty site indicated in inset (b) of Figure 2.

In Table I, we report three contributions to the ionization potential (IP) of the single water molecule when it is inserted in cubic simulation cells of lattice constant a of 4, 6 and 10 Å. The three contributions are defined as follows:

- *Isolated*: The ionization potential of the water molecule is evaluated in the absence of the interaction with its periodic images. In practice, this is achieved employing the Martyna-Tuckerman[3] method.

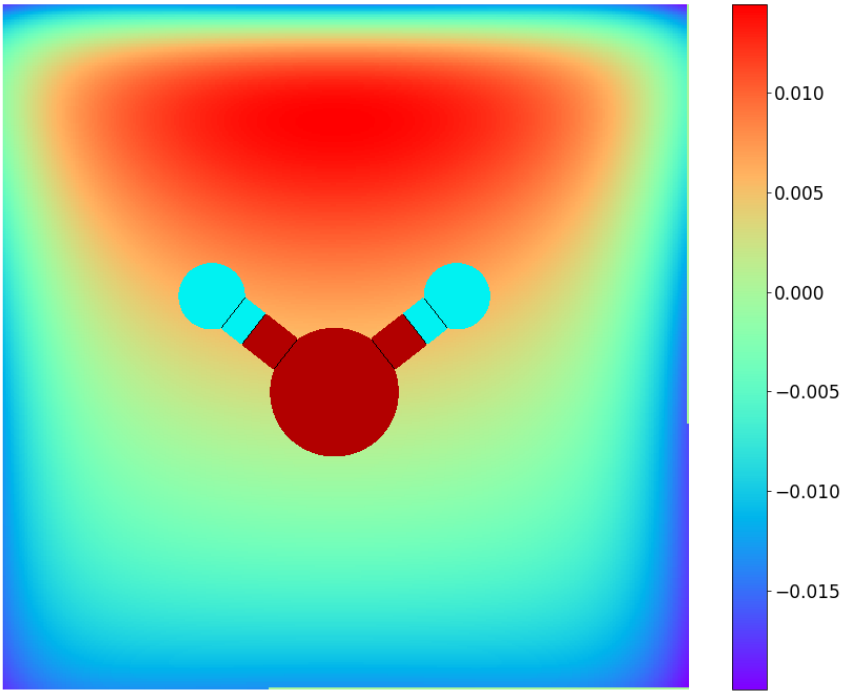

FIG. 3. Depiction of the screening potential, $v^{\text{screen}}(\mathbf{r})$, associated with a single water molecule in a cubic simulation cell with $a = 6$Å.

- *Polarization*: Contribution to the IP from the polarization of the water electron density due to the interaction with its periodic images.

- *Interaction*: Contribution to the IP due to the interaction of the water with its periodic images.

The trend of the three contributions to the water IP follow the expected trend. I.e., as the auxiliary simulation cell increses in size, the interaction of the water molecule with its periodic images weakens. Already at $a = 10$Å, the effect of the interaction on the water electron density is essentially negligible. While the effect on the IP is still significant due to the long-range nature of the interactions involved.

TABLE I. The ionization potetential in eV of a single water molecule embedded by replicas of itself generated by the PBC at varying cubic lattice constants (4, 5, and 10 Å).

Contributions to IP	$a = 4\mathring{A}$	$a = 6\mathring{A}$	$a = 10\mathring{A}$
Isolated	12.903	13.547	13.729
Polarization	-0.012	-0.002	10^{-5}
Interaction	-1.296	-0.837	-0.120
Total IP	11.594	12.707	13.609

B. Bulk water and its ionization potential

We computed vertical IPs for one snapshot of water 64 (i.e., 64 water molecules in a cubic box reproducing the density of the liquid) which was selected randomly from a *ab initio* molecular dynamics (MD) based on subsystem DFT that was carried out previously[27]. The IPs were calculated in three ways: *Isolated*, the molecular geometries were borrowed from the MD and each molecule was computed separately and treated as isolated; *Embedded*: we employed the impurity method describe above and associated Method II to evaluate the interaction energy. The Coulomb kernel of the $\rho - \rho_I$ extended, neutral system (which is common between neutral and ionized states), was taken as reference; *Embedded non-SC*: Same as *Embedded* but the extended subsystem is kept frozen in the calculation of the cationic specie to the one computed for the neutral specie.

Our results on the IP of bulk liquid water is summarized in Figure 4. From the figure we evince that the histogram of IPs for isolated water molecules (computed with the very same geometries as the liquid but considering each water molecule to be isolated) is peaked around the average and only spreads by about 0.1 eV.

The histogram for the IPs of water molecules embedded in the liquid are much broader than the case of isolated water molecules. The IP spread for liquid water is found to be about 2 eV, or 20 times larger than the spread calculated for gas phase water molecules. This is consistent with similar findings for the optical spectrum of water[28–31], where the environment has the effect of broadening the spectrum to the point that the Urbach tail of the liquid is red shifted compared to the gas phase despite the fact that the first band in the liquid peaks at higher energies than the gas phase. In this work, we find a similar behavior, in this case, for the IP distribution.

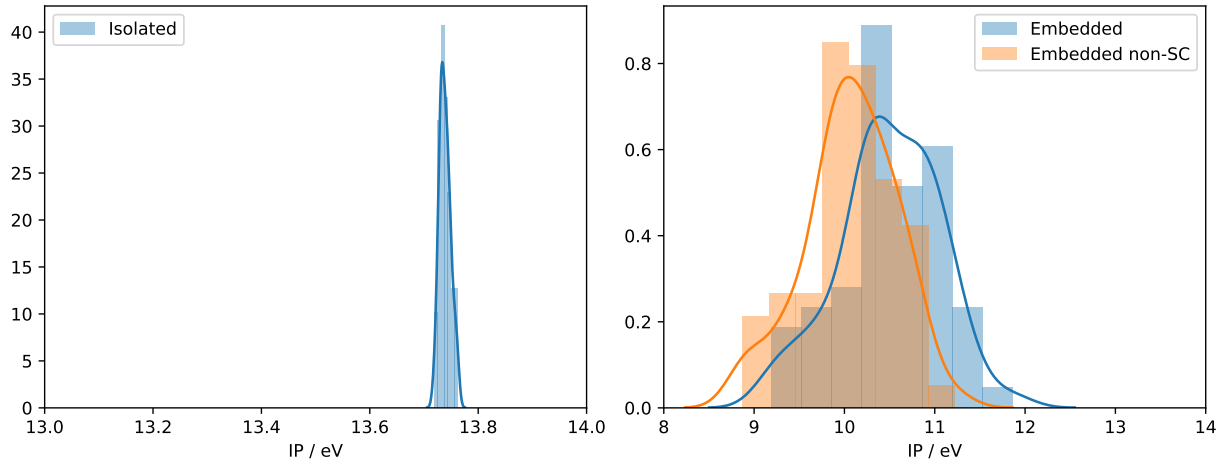

FIG. 4. Distribution of IPs of bulk liquid water. Left: isolated water molecules. Right: Embedded water molecules in the bulk. The "Embedding non-SC" stands for non-selfconsistent embedding (i.e., the embedding potential was computed from the environment of the neutral water molecule). The "Embedding" label stands for selfconsistent embedding potential for the neutral water molecule as well as the cation water.

We summarize the computed average IP of liquid water in Table II. There, we also compare the result we obtain from embedding from the result obtained from a calculation of a water molecule embedded in a continuum dielectric *via* the COSMO model[32].

The computed IPs compare well with recent GW calculations[4] carried out with classical nuclei. While the discrepancy against the IP computed with quantum nuclei (*via* a path-integral dynamics) is of about 0.2 eV. The COSMO values are higher than the computed average. In principle, as the IPs presented here are vertical (i.e., no nuclear relaxation is accounted for in the cationic state) it is difficult to determine the appropriate ϵ to use in COSMO. Thus, we provide the reader with three choices, $\epsilon = 1.8$ representing the response of only the electrons in water, and then two additional higher dielectric constants.

We note that the non selfconsistency in the impurity screening potential has a significant effect on the IP shifting the IP by about 0.4 eV. Thus, in future calculations of the IP of molecular subsystems embedded by extended subsystems will need to include selfconsistency in the screening potential used to generate the impurity model.

TABLE II. The average vertical ionization potetential in eV of liquid water in comparison to recent literature values and COSMO carried out with several effective dielectric constants, ϵ. Liquid GW A/B: IP average form *ab initio* MD involving classical/quantum nuclei.

Gas phase	13.74
Liquid	10.50
Liquid non-SC	10.07
Liquid Exp[33]	9.9
Liquid Exp[34]	10.06
Liquid GW A[4]	10.55
Liquid GW B[4]	10.25
COSMO ($\epsilon = 1.8$)	11.94
COSMO ($\epsilon = 3$)	11.15
COSMO ($\epsilon = 10$)	10.13

V. CONCLUSIONS

In sum, leveraging a density embedding description of the electronic structure of a system in periodic boundary conditions, we were able to define appropriate impurity models that can embed finite neutral and charged subsystems inside an extended (infinite) surrounding subsystem. We call v^{screen} the potential term that realizes the impurity model.

The combination of the impurity model and an appropriate, consistent choice of the reference for Coulomb interactions led us to compute the ionization potential of liquid water. The average value that we compute is 10.5 eV which compares quite well with experiments (9.9–10.06 eV) and very recent simulations based on the GW approximation (10.55 eV). Similar to the optical spectrum of liquid water compared to the gas phase, we find that the IP distribution of liquid water is much broader than the one of gas phase water.

Future vanilla applications of the method will involve ionic crystals – a class of systems where the Madelung fields are very large so that the boundary of applicability of the method are tested. Even less straightforward applications are inspired by the work of Carter and coworkers[35–37] and others[38] will involve employing wavefunction methods for the computation of charged and neutral finite subsystems surrounded by extended subsystems.

VI. ACKNOWLEDGMENTS

This material is based upon work supported by the U.S. Department of Energy, Office of Basic Energy Sciences, under Award Number DE-SC0018343. We are indebted to Christoph Jacob for entartaining discussions on this topic during his visit at Rutgers. We thank Alessandro Genova for guidance in the eQE coding.

REFERENCES

[1]R. Resta and D. Vanderbilt, "Theory of polarization: A modern approach," in *Physics of Ferroelectrics: a Modern Perspective, Topics in Applied Physics*, Vol. 105 (Springer-Verlag, 2007) p. 31.

[2]C. G. V. de Walle and J. Neugebauer, "First-principles calculations for defects and impurities: Applications to III-nitrides," J. Appl. Phys. **95**, 3851–3879 (2004).

[3]G. J. Martyna and M. E. Tuckerman, "A reciprocal space based method for treating long range interactions in ab initio and force-field-based calculations in clusters," J. Chem. Phys. **110**, 2810–2821 (1999).

[4]A. P. Gaiduk, T. A. Pham, M. Govoni, F. Paesani, and G. Galli, "Electron affinity of liquid water," Nature Communications **9** (2018), 10.1038/s41467-017-02673-z.

[5]C. G. V. de Walle and R. M. Martin, "Theoretical study of band offsets at semiconductor interfaces," Phys. Rev. B **35**, 8154–8165 (1987).

[6]Z. Guo, F. Ambrosio, W. Chen, P. Gono, and A. Pasquarello, "Alignment of redox levels at semiconductor–water interfaces," Chem. Mater. **30**, 94–111 (2017).

[7]R. T. Tung and L. Kronik, "Band offset formation at semiconductor heterojunctions through density-based minimization of interface energy," Phys. Rev. B **94** (2016), 10.1103/physrevb.94.075310.

[8]Y. Hinuma, A. Grneis, G. Kresse, and F. Oba, "Band alignment of semiconductors from density-functional theory and many-body perturbation theory," Phys. Rev. B **90** (2014), 10.1103/physrevb.90.155405.

[9]J. Le, M. Iannuzzi, A. Cuesta, and J. Cheng, "Determining potentials of zero charge of metal electrodes versus the standard hydrogen electrode from density-functional-theory-based molecular dynamics," Phys. Rev. Lett. **119** (2017), 10.1103/physrevlett.119.016801.

[10]L. Gao, J. Souto-Casares, J. R. Chelikowsky, and A. A. Demkov, "Orientation dependence of the work function for metal nanocrystals," J. Chem. Phys. **147**, 214301 (2017).

[11]I. Dabo, B. Kozinsky, N. E. Singh-Miller, and N. Marzari, "Electrostatics in periodic boundary conditions and real-space corrections," Phys. Rev. B **77** (2008), 10.1103/physrevb.77.115139.

[12]G. Makov and M. C. Payne, "Periodic boundary conditions in ab-initio calculations," Phys. Rev. B **51**, 4014–4022 (1995).

[13]C. Freysoldt, J. Neugebauer, and C. G. V. de Walle, "FullyAb InitioFinite-size corrections for charged-defect supercell calculations," Phys. Rev. Lett. **102** (2009), 10.1103/physrevlett.102.016402.

[14]O. Andreussi and N. Marzari, "Electrostatics of solvated systems in periodic boundary conditions," Phys. Rev. B **90** (2014), 10.1103/physrevb.90.245101.

[15]T. A. Wesolowski, S. Shedge, and X. Zhou, "Frozen-Density Embedding Strategy for Multilevel Simulations of Electronic Structure," Chem. Rev. **115**, 5891–5928 (2015).

[16]A. Krishtal, D. Sinha, A. Genova, and M. Pavanello, "Subsystem Density-Functional Theory as an Effective Tool for Modeling Ground and Excited States, their Dynamics, and Many-Body Interactions," J. Phys.: Condens. Matter **27**, 183202 (2015).

[17]C. R. Jacob and J. Neugebauer, "Subsystem density-functional theory," WIREs: Comput. Mol. Sci. **4**, 325–362 (2014).

[18]T. A. Wesolowski, "One-Electron Equations for Embedded Electron Density: Challenge for Theory and Practical Payoffs in Multi-Level Modeling of Complex Polyatomic Systems," in *Computational Chemistry: Reviews of Current Trends*, Vol. 10, edited by J. Leszczynski (World Scientific, Singapore, 2006) pp. 1–82.

[19]Here we assume that the periodic density ρ is chosen to be neutral.

[20]T. Laino, F. Mohamed, A. Laio, and M. Parrinello, "An efficient real space multigrid QM/MM electrostatic coupling," J. Chem. Theory Comput. **1**, 1176–1184 (2005).

[21]N. D. M. Hine, J. Dziedzic, P. D. Haynes, and C.-K. Skylaris, "Electrostatic interactions in finite systems treated with periodic boundary conditions: Application to linear-scaling density functional theory," J. Chem. Phys. **135**, 204103 (2011).

[22]N. A. Baker, P. H. Hnenberger, and J. A. McCammon, "Polarization around an ion in a dielectric continuum with truncated electrostatic interactions," J. Chem. Phys. **110**, 10679–10692 (1999).

[23]T. N. Heinz and P. H. Hnenberger, "Combining the lattice-sum and reaction-field approaches for evaluating long-range electrostatic interactions in molecular simulations," J. Chem. Phys. **123**, 034107 (2005).

[24]A. Genova, D. Ceresoli, A. Krishtal, O. Andreussi, R. DiStasio Jr., and M. Pavanello, "eQE — A Densitiy Functional Embedding Theory Code For The Condensed Phase," Int. J. Quantum Chem. **117**, e25401 (2017).

[25]J. P. Perdew, K. Burke, and M. Ernzerhof, "Generalized Gradient Approximation Made Simple," Phys. Rev. Lett. **77**, 3865–3868 (1996).

[26]S. Laricchia, E. Fabiano, L. A. Constantin, and F. Della Sala, "Generalized Gradient Approximations of the Noninteracting Kinetic Energy from the Semiclassical Atom Theory: Rationalization of the Accuracy of the Frozen Density Embedding Theory for Nonbonded Interactions," J. Chem. Theory Comput. **7**, 2439–2451 (2011).

[27]A. Genova, D. Ceresoli, and M. Pavanello, "Avoiding Fractional Electrons in Subsystem DFT Based Ab-Initio Molecular Dynamics Yields Accurate Models For Liquid Water and Solvated OH Radical," J. Chem. Phys. **144**, 234105 (2016).

[28]S. K. P., A. Genova, and M. Pavanello, "Cooperation and environment characterize the low-lying optical spectrum of liquid water," J. Phys. Chem. Lett. **8**, 5077–5083 (2017).

[29]X. Blase, P. Boulanger, F. Bruneval, M. Fernandez-Serra, and I. Duchemin, "GW and Bethe-Salpeter study of small water clusters," J. Chem. Phys. **144**, 034109 (2016).

[30]A. Hermann, W. G. Schmidt, and P. Schwerdtfeger, "Resolving the Optical Spectrum of Water: Coordination and Electrostatic Effects," Phys. Rev. Lett. **100** (2008).

[31]P. H. Hahn, W. G. Schmidt, K. Seino, M. Preuss, F. Bechstedt, and J. Bernholc, "Optical Absorption of Water: Coulomb Effects versus Hydrogen Bonding," Phys. Rev. Lett. **94**, 037404 (2005).

[32]A. Klamt and G. Schüürmann, "COSMO: a new approachto dielectric screening in solvents with explicit expressions for the screening energy and its gradient," J. Chem. Soc. Perk. Trans. 2 , 799–805 (1993).

[33]B. Winter, R. Weber, W. Widdra, M. Dittmar, M. Faubel, and I. V. Hertel, "Full valence band photoemission from liquid water using EUV synchrotron radiation," J. Phys. Chem. A **108**, 2625–2632 (2004).

[34]P. Delahay and K. V. Burg, "Photoelectron emission spectroscopy of liquid water," Chem. Phys. Lett. **83**, 250–254 (1981).

[35]F. Libisch, C. Huang, P. Liao, M. Pavone, and E. A. Carter, "Origin of the Energy Barrier to Chemical Reactions of O_2 on Al(111): Evidence for Charge Transfer, Not Spin Selection," Phys. Rev. Lett. **109**, 198303 (2012).

[36]K. Yu, F. Libisch, and E. A. Carter, "Implementation of density functional embedding theory within the projector-augmented-wave method and applications to semiconductor defect states," J. Chem. Phys. **143**, 102806 (2015).

[37]N. Govind, Y. A. Wang, A. J. R. da Silva, and E. A. Carter, "Accurate ab initio energetics of extended systems via explicit correlation embedded in a density functional environment," Chem. Phys. Lett. **295**, 129–134 (1998).

[38]D. V. Chulhai and J. D. Goodpaster, "Projection-based correlated wave function in density functional theory embedding for periodic systems," Journal of Chemical Theory and Computation **14**, 1928–1942 (2018).